Microelectronics Journal 108 (2021) 104960

Contents lists available at ScienceDirect

Microelectronics Journal

journal homepage: www.elsevier.com/locate/mejo

Shunt resistance spatial variations in amorphous silicon solar cells

Issa Etier [a], Anas Al Tarabsheh [a,b], Nithiyananthan Kannan [c,*]

[a] Electrical Engineering Department, The Hashemite University, Jordan
[b] Electrical and Computer Engineering Department, Abu Dhabi University, Abu Dhabi, United Arab Emirates
[c] Electrical Engineering Department, Faculty of Engineering, Rabigh, King Abdulaziz University, Jeddah, Saudi Arabia

ARTICLE INFO

Keywords:
PV Cells
CV Characteristics
Shunt resistance

ABSTRACT

This article describes the spatial variations of the shunt resistance in a-Si:H, PV cells across the absorber layer (i-layer). When the a-Si:H PV cell is illuminated through its front layer, photo generated carriers distribute along the i-layer as a function of the radiation WL and the voltage drop across the PV cell. The generated electric currents of the electrons and holes are simultaneously determined by solving the equations of the transport, Poisson, and the continuity as a role of the voltage and the place near the i-layer. In this work, leakage flow of electrons and holes is calculated through the i-layer to calculate the corresponding two J/V curves of the two carrier types. Therefore, the shunt resistance associated to each carrier type varies is calculated separately and will be variable overall the i-layer. This research bring out with the calculation of area dependent shunt resistance extracted from the location-dependent J/V curves of the carriers is comparable to the conventional single valued shunt resistance found from the global J/V curve of the PV cell. This proposed work is a novel idea, which clearly indicates the simple technique to calculate shunt resistance spatial variations of a-Si:H PV cell. This article also presents the impact of the CM values on the calculated shunt resistance of the PV cells.

1. Introduction

The (a-Si:H) and solar cells have been improved in the last decade as a result of the progress of the research of their materials and the design [1,2]. The a-Si:H photovoltaic (PV) cells show lower processing cost compared to other PV technologies. This can be attributed to their low deposition temperatures [3,4] which is suitable for flexible plastic substrates. In addition they possess high absorption coefficient and stabilized efficiency values under high operating temperatures. The main motivation for the choice of the a-Si:H PV cells are they are highly bendable, and comparatively less susceptible to cracks than traditional panels constructed from solid wafers of silicon. The a-Si:H semiconductors have interesting optoelectronic properties where they tend to behave like direct band gap semiconductors [5] since they have high absorption coefficient that can be prescribed by the random nature of the atomic ordering. Therefore, localized defects show up which lead to charge leak through the i-layer, which in turn makes the i-layer, which is considered the active layer. The main parameters that describe the performance of PV cells are based on the sc amps (I_{sc}), oc voltage (V_{oc}), factor of fill (FF), and the overall efficiency (η). The aforementioned parameters decease as the shunt resistance R_{sh} decreases [6,7], as depicted in Figs. 1 and 2. The J/V characteristics are clearly affected by the rise in the parallel leakage amperes (i.e the decease of the parallel resistance) which reduces mainly the fill factor, open-circuit voltage, and the efficiency. To calculate the effect of the shunt resistance, we introduced the shunt resistance coefficient of all the affected parameters. Table 1 show the shunt resistance coefficient of the aforementioned parameters where the main effect is on the fill factor rather than the open-circuit voltage.

To describe how much the PV cell parameters respond to the change of the shunt resistance, this paper introduces the shunt resistance coefficients β_{Voc}, β_{FF}, β_{η} of the oc voltage, factor of fill, and the overall efficiency, respectively. Table 1 shows the parallel resistance coefficient of the aforementioned parameters where the main effect is on the fill factor and consequently on the efficiency rather than the open-circuit voltage. To describe how much the PV cell parameters respond to the change of the shunt resistance, this paper introduces the shunt resistance coefficients $\beta_{Voc}, \beta_{FF}, \beta_{\eta}$ of the oc voltage, factor of fill, and the overall efficiency, respectively. Table 1 shows the parallel resistance coefficient of the aforementioned parameters where the main effect is on the fill factor and consequently on the efficiency rather than the open-circuit voltage.

* Corresponding author.
E-mail addresses: etier@hu.edu.jo (I. Etier), anas.altarabsheh@adu.ac.ae (A.A. Tarabsheh), nmajaknap@kau.edu.sa (N. Kannan).

https://doi.org/10.1016/j.mejo.2020.104960
Received 10 September 2020; Received in revised form 27 November 2020; Accepted 1 December 2020
Available online 18 December 2020
0026-2692/

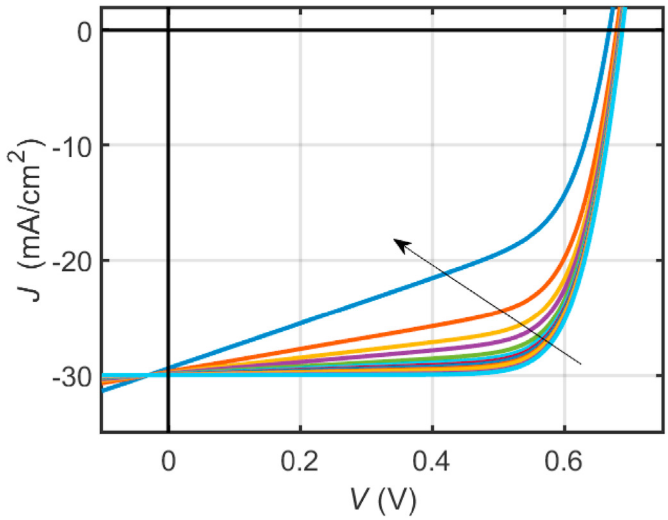

Fig. 1. Shunt resistance effects.

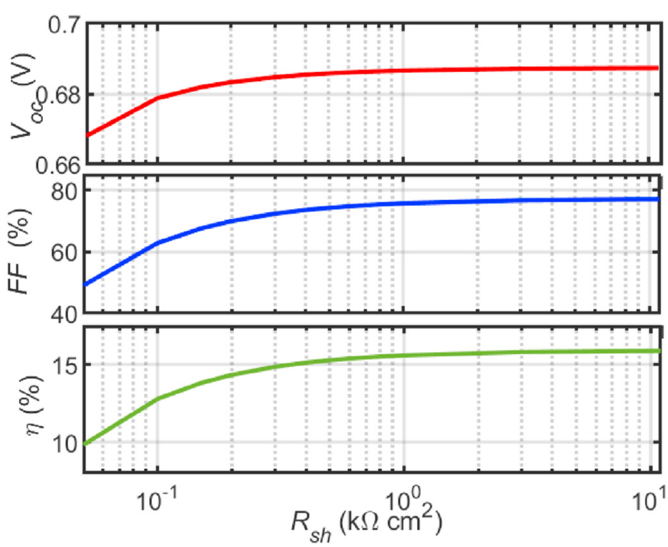

Fig. 2. Effect of the shunt resistance R_{sh} on the open-circuit voltage, fill factor, and the efficiency.

Table 1
Shunt resistance coefficients calculated from Fig. 2.

Shunt resistance Coefficient of V_{oc}: $\boldsymbol{\beta_{Voc}=\Delta V_{oc}/\Delta R_{sh}\cdot 1/V_{oc}\times 100}$	0.27%/kΩ.cm^2
Shunt resistance Coefficient of *FF*: $\boldsymbol{\beta_{FF}=\Delta FF/\Delta R_{sh}\cdot 1/FF\times 100}$	5.21%/kΩ.cm^2
Shunt resistance Coefficient of $\boldsymbol{\eta}$: $\boldsymbol{\beta_{\eta}=\Delta \eta/\Delta R_{sh}\cdot 1/\eta\times 100}$	5.63%/kΩ.cm^2

The following J/V equation of a-Si:H PV cells is used to extract all the needed electrical parameters of the cell:

$$J = J_0\left(exp\left(\frac{V-JR_s}{n_{id}V_t}\right)-1\right)+\left(\frac{V-JR_s}{R_{sh}}\right)-J_{ph} \tag{1}$$

Where V_t is the voltage of thermal effect, n_{id} is the factor of ideality, J_{ph} is approximately the short-circuit current-intensity, R_{sh} is the parallel resistance, R_s is the series resistance, and J_0 is the peak current intensity. The shunt resistance is evaluated from the linear fitting of the current around $V = 0$ V and finding the slope accordingly. The parallel leakage amps in a-Si:H PV cells is prescribed by the drift currents and the minor holes through the i-layer during the fabrication processes.

2. Analysis

The basic AS solar cell has important layers developed as pip or nip structure. The layers are a narrow to the core of twenty nm and p layers are of 100 nm which is bigger in size, intrinsic layer is (i) layer and a very narrow n-type layer. This paper extends the work of our previous conference paper in where the test a-Si:H PV cell is constructed by the PECVD at $r_f = 13.56$ MHz on TCO imprinted glass at 180 °C. The optical properties of the cell are measured by the ellipsometry setup. The p-layer has a wide gap of band and a super conductivity and is deposited directly on the TCO layer. The wide band gap semiconductor results in a large built-in potential and enhances the absorption of the i-layer. The electric field extends to the i-layer, it differentiates the photo-generated electron-hole couple to be received at the front and back layers. Fig. 3 indicates the elevation and section of the test a-Si:H solar cell where the p-layer is collected on the TCO material which has to have both high transparency and conductivity. The structure of the cell has the p-i-n order where the sun light enters the p-layer region.

The optical specifications of both the layers are optimized to maximize the absorption constant α in the visible solar spectrum. To absorption constant α is measured by the ultraviolet-to-infrared spectrophotometer in the wavelength ranges between 400 nm and 2000 nm. Fig. 4 shows the measured absorption constant α for the two the p- and the i-layers.

3. Discussion and results

This work relies on the differential derivations of the system, used by the author Tarabsheh, it solves the continuity and Poisson equations of the electrons and holes simultaneously. Thus, the system comes out with three solutions for the amps voltage characteristics of all the carriers. In the forward-bias region of the current voltage characteristic, the shunt resistance R_{sh} results in unwanted current at low bias voltages, known as shunt leakage current, while the series resistance R_s limits the current at higher voltage values. The rise of the parallel leakage current or the decrease in R_{sh} decreases the current at the voltage values less than the voltage $V_m at$ the maximum power, and reduces the fill factor and the efficiency as shown in Fig. 2. The presence of the series resistance R_s reduces the generated current of the cell for $V \geq V_m$. The shunt resistances due to the electrons, holes, and the total carriers are evaluated as $R_{sh,n} = \frac{dV}{dJ_n}, R_{sh,p} = \frac{dV}{dJ_p}, andR_{sh} = \frac{dV}{dJ}$, respectively, by linearly fitting the J/V curves around $V = 0$. The continuity equations for the minority carriers in the p-type and the minority carriers in the n-type, respectively, are be expressed as:

$$\frac{d^2n(x,\lambda)}{dx^2}+E\frac{\mu_n}{D_n}\frac{dn(x,\lambda)}{dx}-\frac{n(x,\lambda)}{D_n\tau_n} = -\left[\frac{N_D}{D_n\tau_n}e^{\frac{V_{bi}W}{V_t(x-W)}}+\frac{G(x,\lambda)}{D_n}\right] \tag{2}$$

$$\frac{d^2p(x,\lambda)}{dx^2}+E\frac{\mu_p}{D_n}\frac{dp(x,\lambda)}{dx}-\frac{p(x,\lambda)}{D_n\tau_n} = -\left[\frac{N_A}{D_p\tau_p}e^{\frac{V_{bi}W}{V_t(x-W)}}+\frac{G(x,\lambda)}{D_p}\right] \tag{3}$$

and

$$E\mu_p\frac{dp(x,\lambda)}{dx}-D_p\frac{d^2p(x,\lambda)}{dx^2} = -\frac{n(x,\lambda)-n_0(x,\lambda)}{\tau_n}+G(x,\lambda) \tag{4}$$

$$E\mu_n\frac{dn(x,\lambda)}{dx}-D_n\frac{d^2n(x,\lambda)}{dx^2} = -\frac{p(x,\lambda)-p_0(x,\lambda)}{\tau_p}+G(x,\lambda) \tag{5}$$

Where $G(\lambda, x)$ is the photo-generation rate in the i-layer which is dependent on the incoming solar spectrum $N_{ph}(\lambda)$ and the absorption constant α, E is the electric voltage inside the layer of i, x is the distance with reference to the p-layer, τ_n is the life of the electron, τ_p is the hole lifetime, μ_n is the electron mobility, D_n is the constant of the diffusion electrons, μ_p is the hole mobility, D_p is the constant diffusion of the holes, N_A is the concentration of the acceptor atoms, N_D is the assembly of the donor atoms, W is the width of the i-layer, V_{bi} is the built-in

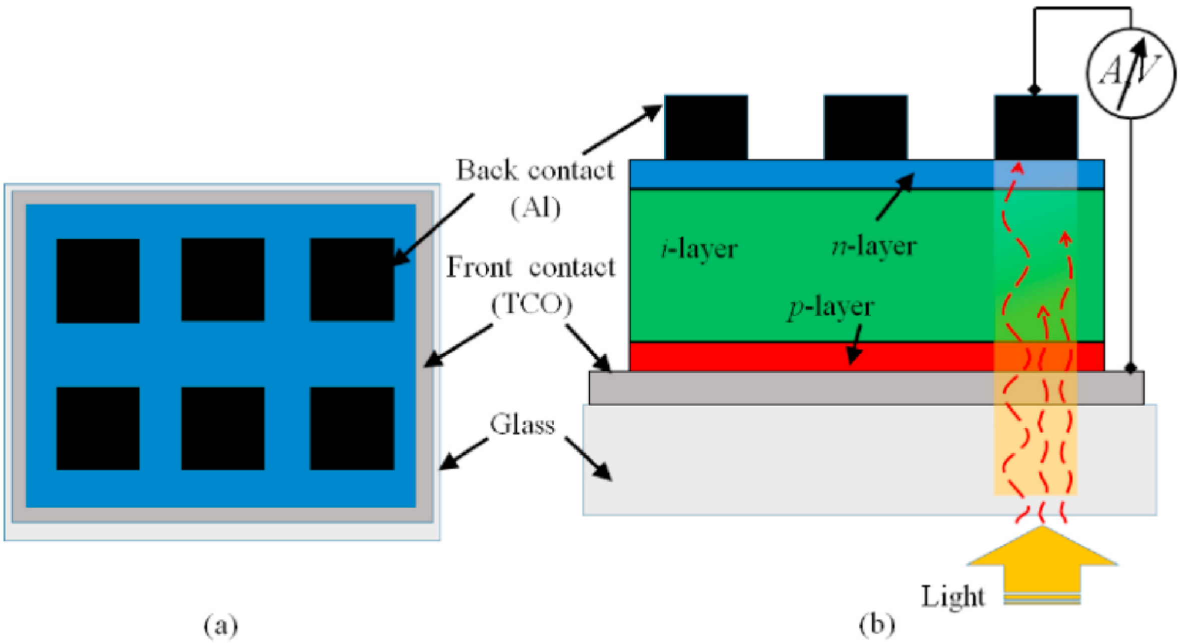

Fig. 3. Top (a) and cross-section (b) views of the test solar cell.

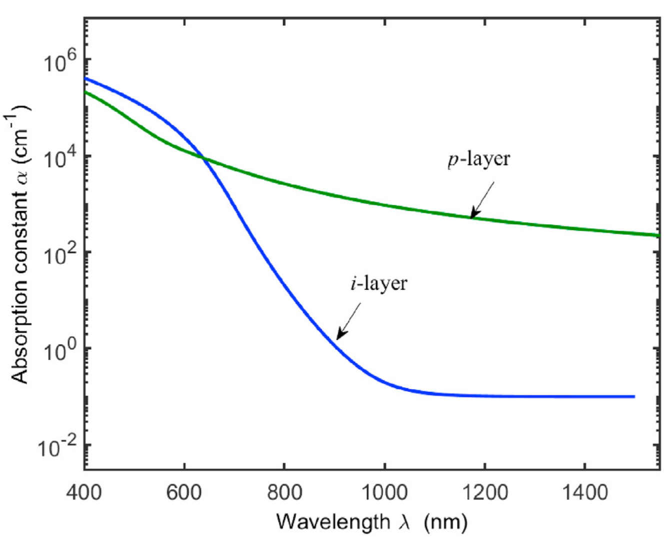

Fig. 4. Absorption Constant α of the p- and i-Layer as a Function of the Wavelength λ of the Solar Spectrum.

potential, and n_0 is the heat equilibrium concentration of the electrons. The solutions for the electron assembly $n(x)$ and the hole assembly $p(x)$ from the aforementioned derivations are depicted in Fig. 5 which proves that the distributions of the electrons and holes vary with varying the wavelength of the solar spectrum. The integration of $n(x)$ and $p(x)$ with respect to wavelength of the solar spectrum results in the total carrier concentration as a function of the position in the i-layer. Fig. 6 depicts the total carrier concentrations in the i-layer of the test PV cell.

The calculation of the current-densities J_n and J_p is implemented by solving the diffusion and the drift equations as follows:

$$J_n(x) = qD_n \frac{dn(x)}{dx} + q\mu_n n(x) E \tag{6}$$

$$J_p(x) = -qD_p \frac{dp(x)}{dx} + q\mu_p p(x) E \tag{7}$$

The summation J_n and J_p equals the total current-density J. The structure of the test cell in this work has the p-i-n structure to utilize the high absorption of the photons in the front (p-) layer as per the Beer's law, and to utilize the fact that the mobility-lifetime product for the holes is less than that of the electrons. Fig. 7 compares the current-density voltage characteristics of the test cell simulated by MATLAB and the experimental data. The good matching between the measurement and the simulation, by applying the fitting parameters as in, validates the used model.

This paper determines both the hole and the electron current intensity, J_p and J_n, at individual position in the i-layer. Therefore, the parallel resistances due to each curve of electrons and the holes, $R_{sh,n}$ and $R_{sh,p}$. The total parallel resistance R_{sh} is determined in the same manner from the total current-density J. An important conclusion from Fig. 8 is that the current densities are position-dependent in the i-layer leading to discrepancy of the calculated shunt resistance values of the electrons and the holes.

The parallel resistance is determined by a linearly fitting the J/V-characteristics like $V = 0$ V. The parallel resistances $R_{sh,n}$, $R_{sh,p}$, and R_{sh} are determined from Fig. 8(c) and (d), and Fig. 7, respectively, and reflected into Fig. 9 which describes the pattern of each shunt type in the i-layer. Calculating the shunt resistance from the total current density curve is comparable to the combination between the shunt resistance due to the electrons and the holes. Fig. 9 shows that the constant values of R_{sh} match the equivalent parallel combination $R_{sh,n}//R_{sh,p}$.

This work also correlated the high shunt resistance with the less values of carriers. The number of the parallel resistances calculated from the simulations of J/V curves depend strongly on the carrier' mobility, which agrees with the work of Wuerfel. Fig. 10 shows that decreasing the carriers' mobility μ_n andμ_p can reduce the shunt resistance in the i-layer. This paper also indicates the lessspecifications of the carrier mobility's by the low shunt resistance of the PV cell. The values of the shunt resistances calculated from the simulated J/V curves depend strongly on the carriers' mobility, which agrees with the work of Wuerfel. Fig. 10 shows that decreasing the carriers' mobility μ_n and μ_p can reduce the shunt resistance in the i-layer. Fig. 10 shows also the impact of the hole mobility values is greater than that of the electrons.

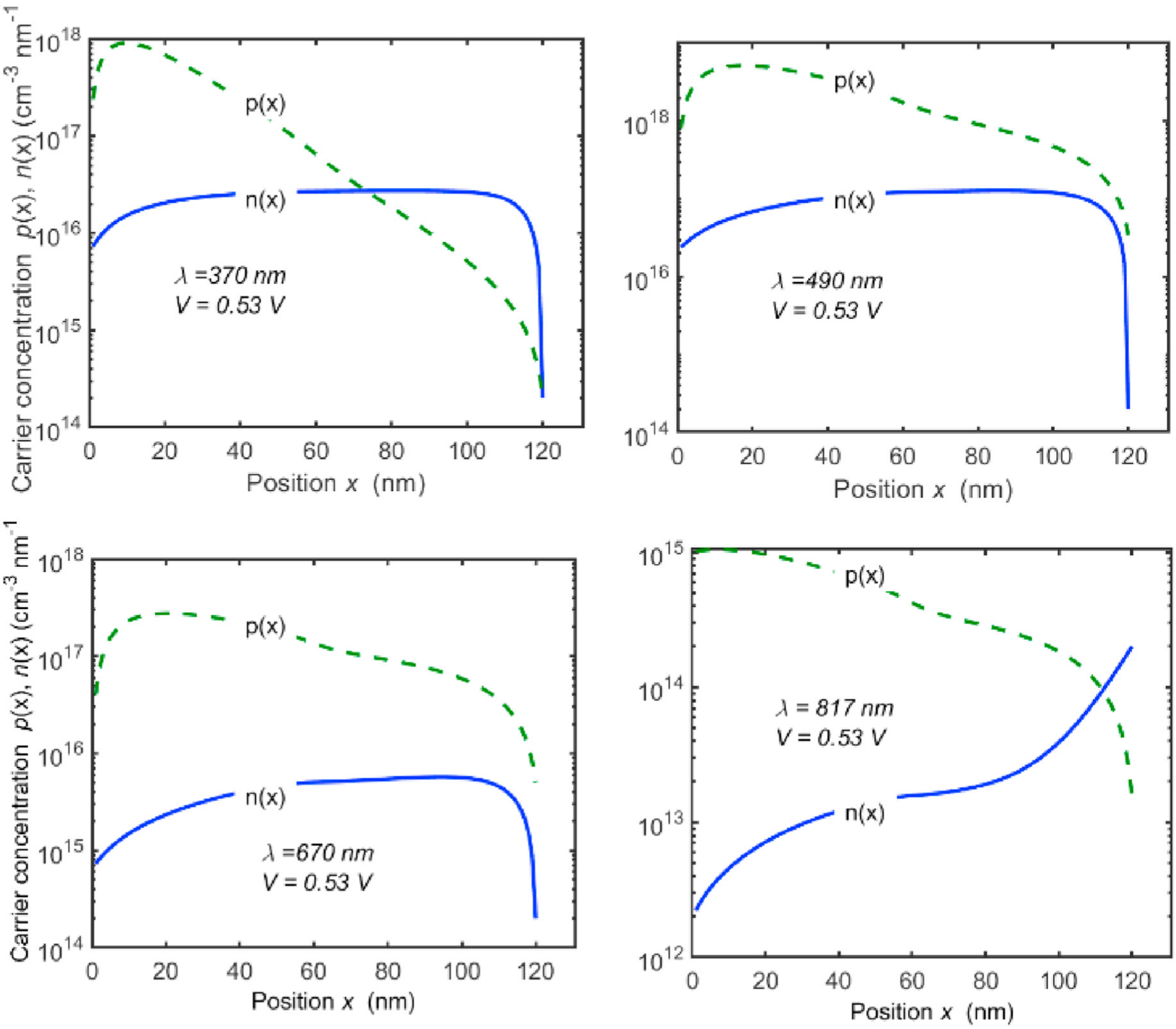

Fig. 5. Photo-Generated Carrier Concentrations of the Holes and the Electrons in the i-Layer of the Test PV Cell at Predefined Applied Voltage of V = 0.53V and Wavelength Values of $\lambda = 370$ nm, … , 817 nm.

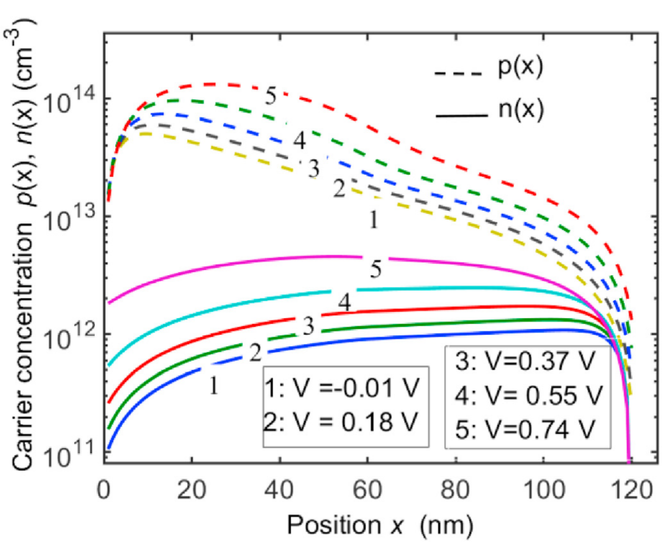

Fig. 6. Carrier concentrations.

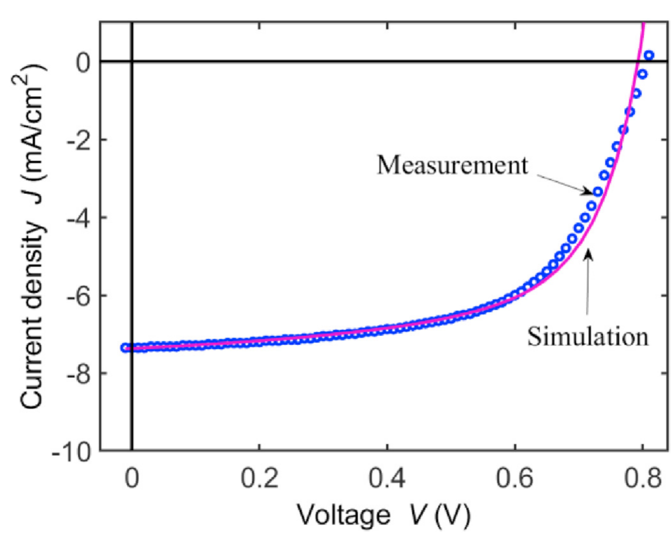

Fig. 7. Current-density voltage of the test cell.

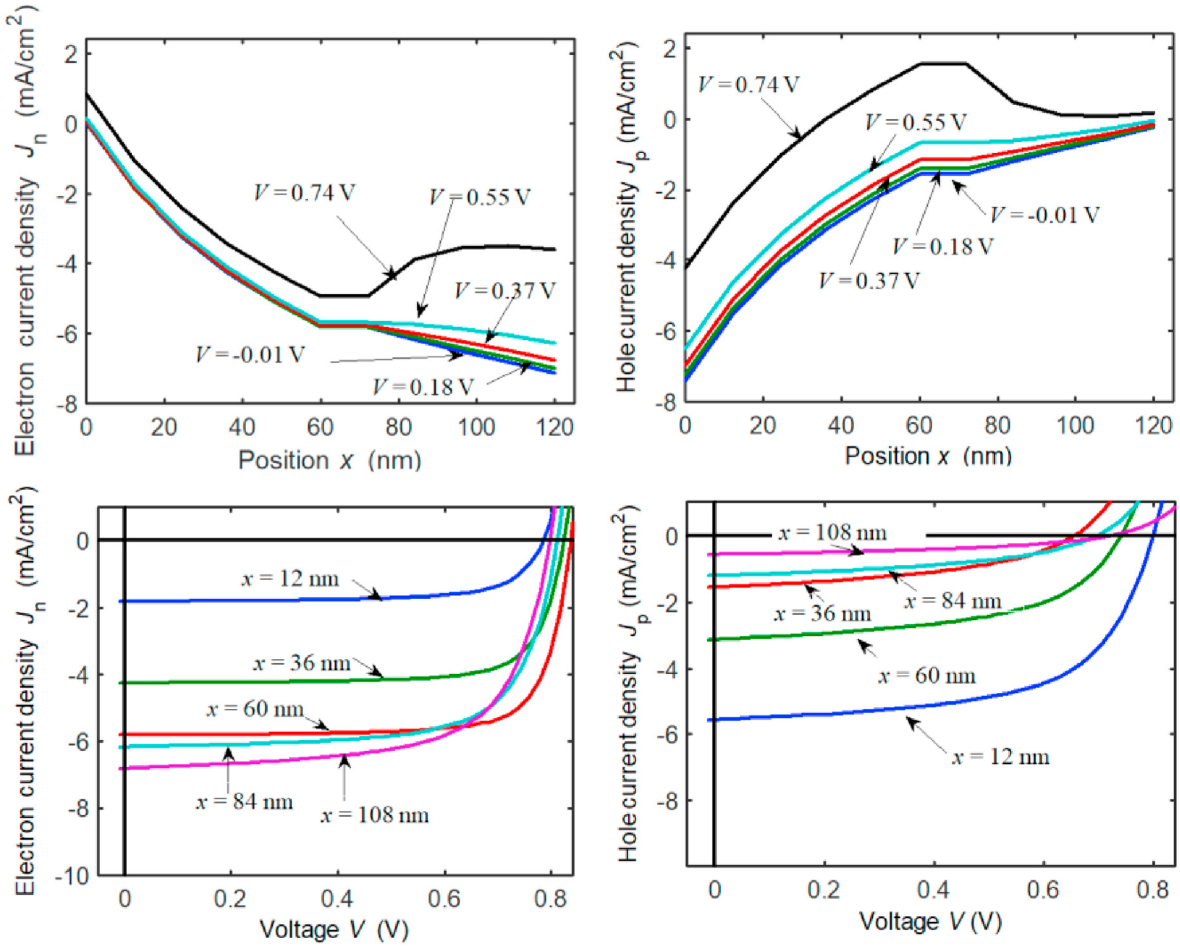

Fig. 8. Electron (a) and Hole (b) Current-Density Curves Versus the Position in the i-Layer, Electron (c) and (d) Hole Current Densities Versus the Voltage Calculated at Different Positions and Different Positions.

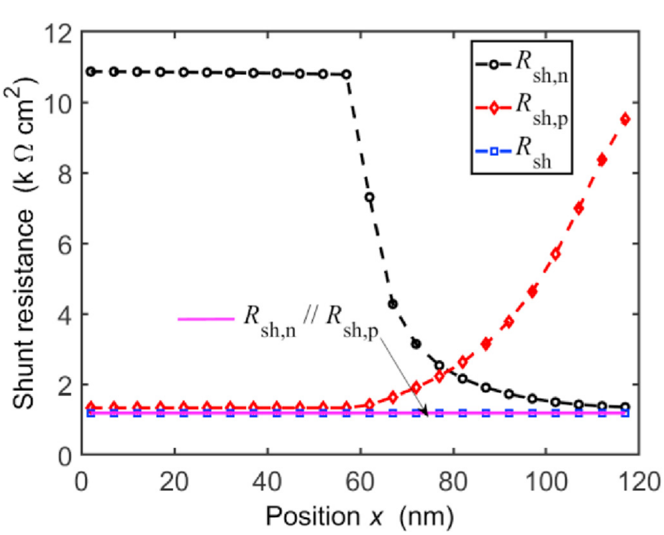

Fig. 9. Variations of shunt resistance.

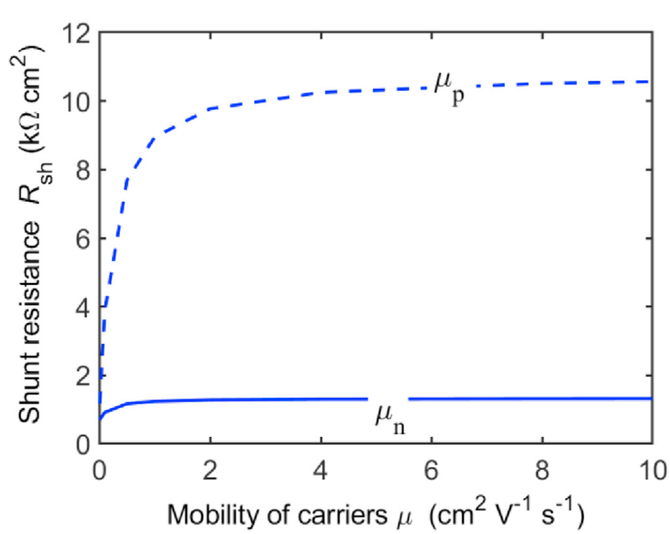

Fig. 10. Shunt Resistance R_{sh} as a Function μ_n and μ_p. The Shunt Resistance is Enhanced for Higher Mobility Values.

4. Conclusion

This work studied the spatial dependence of the electron and hole current-density voltage curves of a-Si:H PV cells in the i-layer. Therefore, the resulting calculated shunt resistance of each carrier type varies across the i-layer. This work indicated that the shunt equivalent combination of the position-based parallel resistances due to the carriers equals match very well the parallel resistance of the cell determined from the total J/V characteristics. This concludes that the parallel resistances implemented in the designed circuit of solar cells are developed of twin parallel-connected parallel resistances; due to the holes and due to the electrons. At the end, this article showed that improving the carriers' mobility's increases the shunt resistance of the PV cell.his proposed research work can be extended in future with different materials such as Copper gallium indium diselenide, Cadmium telluride (CdTe) and Organic photovoltaic cells with different doping level cells. a-Si:H PV panels are yet use extensively in the market due its productive high cost.

CRediT author statement

Nithiyananthan Kannan: Conceptualization, Writing- Original draft preparation, Methodology, Software, Issa Etier: Data curation, Writing-Reviewing and Editing, Validation. Anas Al Tarabsheh: Data curation, Writing- Reviewing and Editing, Validation.

Declaration of competing interest

The authors declare that they have no known competing financial interests or personal relationships that could have appeared to influence the work reported in this paper.

Acknowledgment

The authors acknowledge the research and sponsored programs office in Abu Dhabi University for funding this work under the grant "19300473" and also the Institute for Photovoltaics at University of Stuttgart-Germany for the fabrication of the a-Si:H photovoltaic cells.

References

[1] M. Stuckelberger, R. Biron, N. Wyrsch, F.J. Haug, C. Ballif, Progress in solar cells from hydrogenated amorphous silicon, Renew. Sustain. Energy Rev. 76 (2017) 1497–1523.
[2] J.M. Ball, M.M. Lee, A. Hey, H.J. Snaith, Low-temperature processed meso-superstructured to thin-film perovskite solar cells, Energy *Environ. Sci.* 6 (6) (2013) 1739–1743.
[3] S. Garud, M. Bokalič, C. thi Trinh, B. Rech, D. Amkreutz, M. Topič, Analysis of surface passivation and laser firing on thin-film silicon solar cells via light-beam induced current, IEEE Journal of Photovoltaics 10 (5) (2020) 1246–1253.
[4] S.K. Dargar, V.M. Srivastava, Design and analysis of improved performance amorphous-silicon thin film solar panel, in: 2019 PhotonIcs & Electromagnetics Research Symposium-Spring (PIERS-Spring), IEEE, 2019, pp. 860–866.
[5] M.A. Leilaeioun, W. Weigand, M. Boccard, J.Y. Zhengshan, K. Fisher, Z.C. Holman, Contact resistivity of the p-type amorphous silicon hole contact in silicon heterojunction solar cells, IEEE Journal of Photovoltaics 10 (1) (2019) 54–62.
[6] C. Álvarez-Macías, J.D. Escobar-Carrasquilla, A. Dutt, E. Mon-Pé, L. Gonzé, G. Santana, Development of optimal nanocrystalline absorption layer for thin film silicon solar cell applications, Nano 12 (11) (2017) 1–9.
[7] X. Hu, Y. Wang, Y. Jia, J. Hong, T. Chen, J. Xue, Z. Zhu, Resistive effects on the spatially resolved absolute electroluminescence of thin-film Cu (in, Ga) Se 2 solar cells studied by a distributed two-diode model, IEEE Access 8 (2020) 112859–112866.